

Variations in the Summer Oceanic $p\text{CO}_2$ and Carbon Sink in the Prydz Bay Using the SOM Analysis Approach

Suqing Xu¹, Keyhong Park^{2*}, Yanmin Wang³, Liqi Chen^{1*}, Di Qi¹, Bingrui Li⁴

1. Key Laboratory of Global Change and Marine-Atmospheric Chemistry, Third Institute of Oceanography, Xiamen 361005, PR China.
2. Division of Polar Ocean Sciences, Korea Polar Research Institute, Incheon 21990, South Korea.
3. Haikou Marine Environment Monitoring Central Station, State Oceanic Administration, Haikou 570100, China.
4. Polar Research Institute of China, Shanghai 200136, China.

Correspondence to: Liqi Chen (chenliqi@tio.org.cn);

Keyhong Park (keyhongpark@kopri.re.kr)

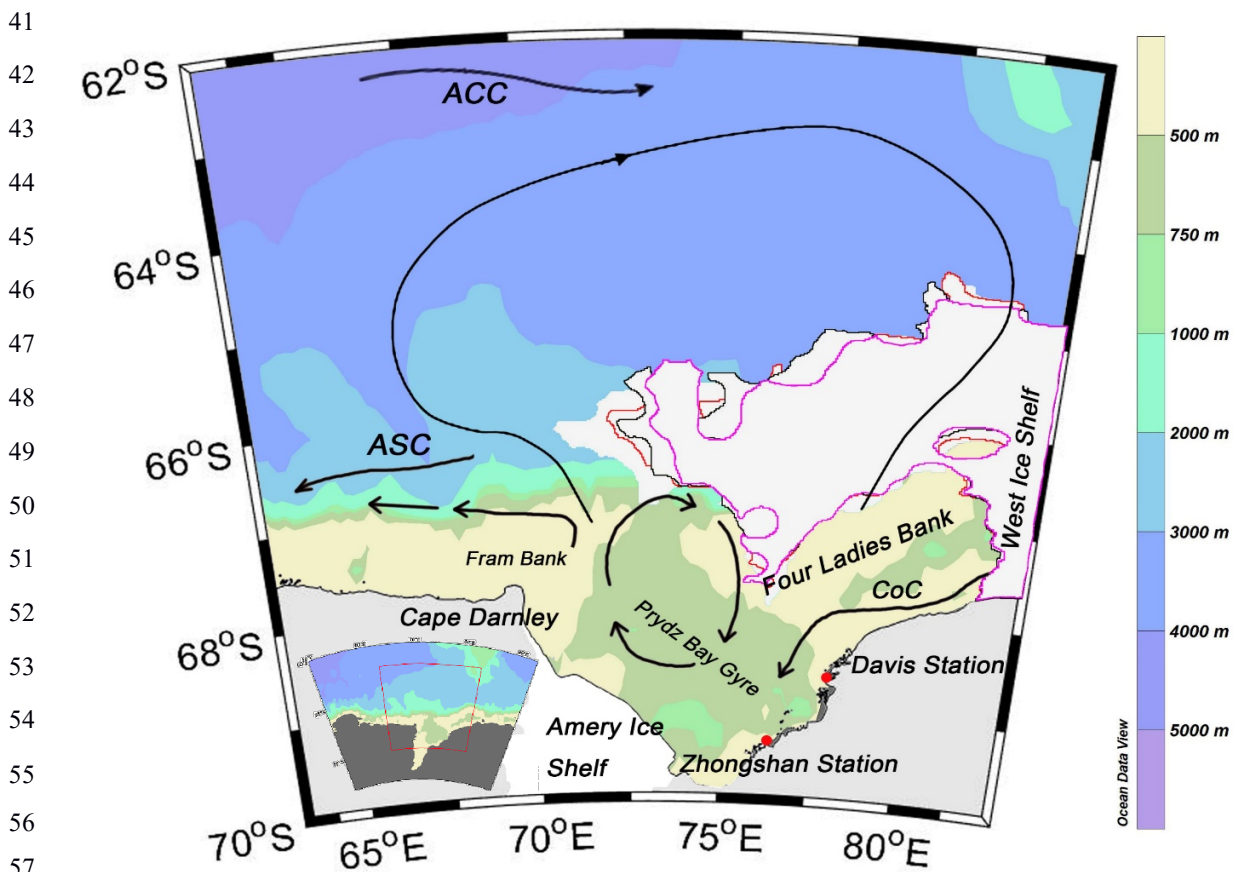
Abstract

This study applies a neural network technique to produce maps of oceanic surface $p\text{CO}_2$ in the Prydz Bay in the Southern Ocean on a weekly 0.1° longitude \cdot 0.1° latitude grid based on in situ measurements obtained during the 31st CHINARE cruise from February to early March of 2015. This study area was divided into three regions, namely, the Open-ocean region, Sea-ice region and Shelf region. The distribution of oceanic $p\text{CO}_2$ was mainly affected by physical processes in the Open-ocean region, where mixing and upwelling were the main controls. In the Sea-ice region, oceanic $p\text{CO}_2$ changed sharply due to the strong change in seasonal ice. In the Shelf region, biological factors were the main control. The weekly oceanic $p\text{CO}_2$ was estimated using a self-organizing map (SOM) with four proxy parameters (Sea Surface Temperature, Chlorophyll-a concentration, Mixed Layer Depth, and Sea Surface Salinity) to overcome the complex relationship between the biogeochemical and physical conditions in the Prydz Bay region. The reconstructed oceanic $p\text{CO}_2$ data coincide well with the in situ investigated $p\text{CO}_2$ data from SOCAT, with a root-mean-square error of $22.14 \mu\text{atm}$. The Prydz Bay was mainly a strong CO_2 sink in February 2015, with a monthly averaged uptake of $23.57 \pm 6.36 \text{ TgC}$. The oceanic CO_2 sink is pronounced in the Shelf region due to its lowest oceanic $p\text{CO}_2$ and peak biological production.

29 **1 Introduction**

30 The amount of carbon uptake occurring in the ocean south of 60°S is still uncertain despite its
31 importance in regulating atmospheric carbon and acting as a net sink for anthropogenic carbon
32 (Sweeney et al., 2000, 2002; Morrison et al., 2001; Sabine et al., 2004; Metzl et al., 2006;
33 Takahashi et al., 2012). This uncertainty arises from both the strong seasonal and spatial variations
34 that occur around Antarctica and the difficulty of obtaining field measurements in the region
35 because of its hostile weather and remoteness.

36 Following the Weddell and Ross seas, the Prydz Bay is the third-largest embayment in the
37 Antarctic continent. Situated in the Indian Ocean section, the Prydz Bay is located close to the
38 Amery Ice Shelf to the southwest and the West Ice Shelf to the northeast, with Cape Darnley to the
39 west and the Zhongshan and Davis stations to the east (Fig. 1). In this region, the water depth
40 increases sharply northward from 200 m to 3000 m.



58 Fig. 1 Ocean circulations in the Prydz Bay derived from Roden et al. (2013), Sun et al. (2013), Wu et al. (2017).
59 ASC: Antarctic Slope Current; CoC: Antarctic Coastal Current; ACC: Antarctic Circumpolar Current. During

60 the 4-week cruise, the sea ice extent varied as indicated by the contoured white areas: the pink line is for
61 week-1(20150202-20150209), the black line is for week-2 (20150210-20150217), the red line is for the week-3
62 (20150218-20150225) and a fourth contoured area is for week-4 (20150226-20150305).

63 The inner continental shelf is dominated by the Amery Depression, which mostly ranges in
64 depth from 600 to 700 m. This depression is bordered by two shallow banks (<200 m): the Fram
65 Bank and the Four Ladies Bank, which form a spatial barrier for water exchange with the outer
66 oceanic water (Smith and Trégure, 1994). The Antarctic Coastal Current (CoC) flows westward,
67 bringing in cold waters from the east. When the CoC reaches the shallow Fram Bank, it turns
68 north and then partly flows westward, while some of it turns eastward, back to the inner shelf,
69 resulting in the clockwise-rotating Prydz Gyre (see Fig.1). The circulation to the north of the bay
70 is characterized by a large cyclonic gyre, extending from within the bay to the Antarctic
71 Divergence at approximately 63°S (Nunes Vaz and Lennon, 1996; Middleton and Humphries,
72 1989; Smith et al., 1984; Roden et al., 2013; Wu et al., 2017). The inflow of this large gyre hugs
73 the eastern rim of the bay and favours the onshore intrusions of warmer modified Circumpolar
74 Deep Water across the continental shelf break (Heil et al., 1996). Westward flow along the shelf,
75 which is part of the wind-driven Antarctic Slope Current (ASC), supplies water to the Prydz Bay.

76 It has been reported that the Prydz Bay is a strong carbon sink, especially in the austral
77 summer (Gibson et al., 1999; Gao et al., 2008; Roden et al., 2013). Moreover, studies have
78 shown that the Prydz Bay region is one of the source regions of Antarctic Bottom Water as well
79 as the Weddell and Ross seas (Jacobs and Georgi, 1977; Yabukiet al., 2006). It is thus important
80 to study the carbon cycle in the Prydz Bay. However, the analysis of the temporal variability and
81 spatial distribution mechanism of oceanic $p\text{CO}_2$ in the Prydz Bay is limited to cruises or stations
82 due to its unique physical environment and complicated marine ecosystem (Smith et al., 1984;
83 Nunes Vaz et al., 1996; Liu et al., 2003). To estimate regional sea-air CO_2 fluxes, it is necessary to
84 interpolate between in situ measurements to obtain maps of oceanic $p\text{CO}_2$. Such an interpolation
85 approach, however, is still difficult, as observations are too sparse over both time and space to
86 capture the high variability in $p\text{CO}_2$. Satellites do not measure sea surface $p\text{CO}_2$, but they do
87 provide access to the parameters related to the processes that control its variability. The seasonal
88 and geographical variability of surface water $p\text{CO}_2$ is indeed much greater than that of atmospheric
89 $p\text{CO}_2$. Therefore, the direction of sea-air CO_2 transfer is mainly regulated by oceanic $p\text{CO}_2$, and
90 the method of spatially and temporarily interpolating in situ measurements of oceanic $p\text{CO}_2$ has
91 long been used (Takahashi et al., 2002 and 2009; Olsen et al., 2004; Jamet et al., 2007; Chierici et

92 al., 2009). In earlier studies, a linear regression extrapolation method was applied to expand cruise
93 data to study the carbon cycle in the Southern Ocean (Rangama et al., 2005; Chen et al., 2011; Xu
94 et al., 2016). However, this linear regression relied simply on either chlorophyll-a (CHL) or sea
95 surface temperature (SST) parameters. Thus, this method can not sufficiently represent all
96 controlling factors. In this study, we applied self-organizing map (SOM) analysis to expand our
97 observed data sets and estimate the oceanic $p\text{CO}_2$ in the Prydz Bay from February to early March
98 of 2015.

99 The SOM analysis, which is a type of artificial neural network, has been proven to be a useful
100 method for extracting and classifying features in the geosciences, such as trends in (and between)
101 input variables (Gibson et al., 2017; Huang et al., 2017b). The SOM uses an unsupervised
102 learning algorithm (i.e., with no need for a priori, empirical or theoretical descriptions of
103 input-output relationships), thus enabling us to identify the relationships between the state
104 variables of the phenomena being analysed, where our understanding of these cannot be fully
105 described using mathematical equations and thus where applications of knowledge-based models
106 are limited (Telszewski et al., 2009). In the field of oceanography, SOM has been applied for the
107 analysis of various properties of seawater, such as sea surface temperature (Iskandar, 2010; Liu et
108 al., 2006), and chlorophyll concentration (Huang et al., 2017a; Silulwane et al., 2001). In the past
109 decade, SOM has also been applied to produce basin-scale $p\text{CO}_2$ maps, mainly in the North
110 Atlantic and Pacific Ocean, by using different proxy parameters (Lafevre et al., 2005; Friedrich
111 & Oeschies, 2009a, 2009b; Nakaoka et al., 2013; Telszewski et al., 2009; Hales et al., 2012; Zeng et
112 al., 2015; Laruelle et al., 2017). SOM has been proven to be useful for expanding the
113 spatial-temporal coverage of direct measurements or for estimating properties whose satellite
114 observations are technically limited. One of the main benefits of the neural network method over
115 more traditional techniques is that it provides more accurate representations of highly variable
116 systems of interconnected water properties (Nakaoka et al., 2013).

117 We conducted a survey during the 31st CHINARE cruise in the Prydz Bay (Fig. 2). This study
118 aimed to apply the SOM method, combined with remotely sensed data, to reduce the
119 spatiotemporal scarcity of contemporary $\Delta p\text{CO}_2$ data and to obtain a better understanding of the
120 capability of carbon absorption in the Prydz Bay from 63°E to 83°E and 64°S to 70°S from
121 February to early March of 2015.

122 The paper is organized as follows. Section 2 provides descriptions of the in situ measurements
123 and SOM methods. Section 3 presents the analysis and discussion of the results, and section 4
124 presents a summary of this research.

125 **2 Data and methods**

126 **2.1 In situ data**

127 The in situ underway $p\text{CO}_2$ values of marine water and the atmosphere were collected during
128 the 31st CHINARE cruise, when the R/V Xuelong sailed from east to west from the beginning of
129 February to early March, 2015 (see Fig.2a, b). Sea water at a depth of 5 metres beneath the sea
130 surface was pumped continuously to the GO system (GO Flowing $p\text{CO}_2$ system, General Oceanics
131 Inc., Miami FL, USA), and the partial pressure of the sea surface water was measured by an
132 infrared analyser (LICOR, USA, Model 7000). The analyser was calibrated every 2.5-3 h using
133 four standard gases supplied by NOAA's Global Monitoring Division at pressures of 88.82 ppm,
134 188.36 ppm, 399.47 ppm, and 528.92 ppm. The accuracy of the measured $p\text{CO}_2$ data is within 2
135 μatm (Pierrot et al., 2009). Underway atmospheric $p\text{CO}_2$ data were simultaneously collected by
136 the GO system. The biological and physical pumps in the ocean (Hardman-Mountford et al., 2009;
137 Bates et al., 1998a, 1998b; Barbini et al., 2003; Sweeney, 2002), are the key factors controlling the
138 variation in sea surface $p\text{CO}_2$. In terms of the physical pumps, the solubility of CO_2 is affected
139 by temperature and salinity, but the biological pumps, such as, phytoplankton, take up CO_2
140 through photosynthesis while organisms release it through respiration (Chen et al., 2011). There
141 are several processes that can influence the distribution of oceanic $p\text{CO}_2$.

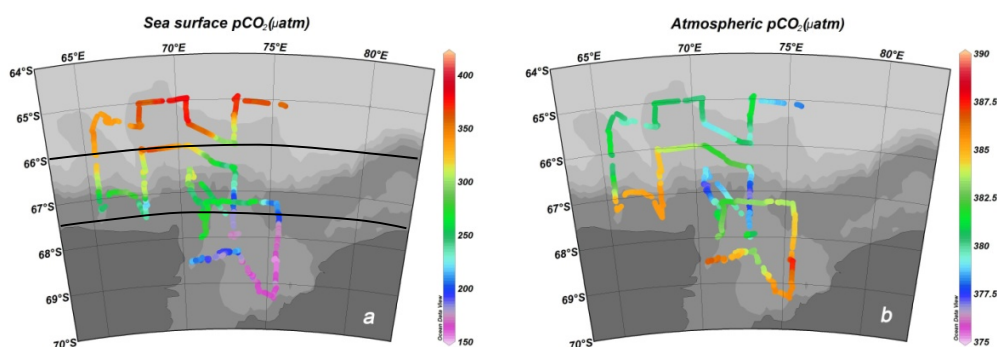
142 Sea ice melt has a significant impact on the local stratification and circulation in polar regions.
143 During freezing, brine is rejected from ice, thereby increasing the sea surface salinity. When ice
144 begins to melt, fresher water is added into the ocean, thereby diluting the ocean water, i.e.,
145 reducing its salinity. Changes in salinity thus record physical processes. In this study, we treat
146 salinity as an index for changes in sea ice. The underway SST and conductivity data were recorded
147 by a Conductivity-Temperature-Depth sensor (CTD, Seabird SBE 21) along the cruise track. Later,
148 sea surface salinity was calculated based on the recorded conductivity and temperature data. The
149 distributions of underway SST and SSS are shown in Fig.2c and d.

150 In austral summer, when sea ice started to melt, ice algae were released into the seawater, and
151 the amount of living biological species and primary productivity increased; thus, high
152 chlorophyll-a values were observed (Liu et al., 2000; Liu et al., 2003). Previous studies have

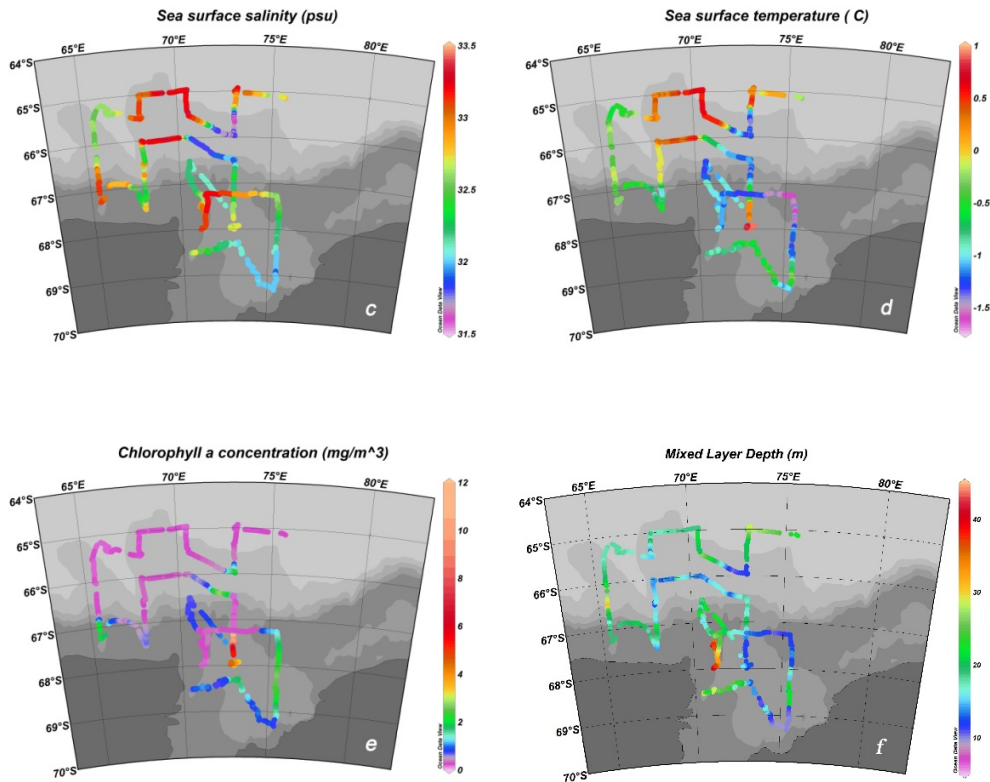
153 reported that the summer sink in the Prydz Bay is biologically driven and that the change in $p\text{CO}_2$
154 is often well correlated with the surface chlorophyll-a concentration (Rubin et al., 1998; Gibsonab
155 et al., 1999; Chen et al., 2011; Xu et al., 2016). The chlorophyll-a value is regarded as an important
156 controlling factor of $p\text{CO}_2$. Remote sensing data of chlorophyll-a obtained from MODIS with a
157 resolution of 4 km (<http://oceancolor.gsfc.nasa.gov>) were interpolated according to the cruise
158 track (Fig.2e).

159 The ocean mixed layer is characterized as having nearly uniform physical properties
160 throughout the layer, with a gradient in its properties occurring at the bottom of the layer. The
161 mixed layer links the atmosphere to the deep ocean. Previous studies have emphasized the
162 importance of accounting for vertical mixing through the mixed layer depth (MLD, Dandonneau,
163 1995; Lüger et al., 2004). The stability and stratification of this layer prevent the upward mixing of
164 nutrients and limit biological production, thus affecting the sea-air CO_2 exchange. Two main
165 methods are used to calculate the MLD (Chu and Fan, 2010): one is based on the difference
166 criterion, and one is based on the gradient criterion. Early studies suggested that the MLD values
167 determined in the Southern Ocean using the difference criterion are more stable (Brainerd and
168 Gregg, 1995; Thomson and Fine, 2003). Thus, following Dong et al. (2008), we calculated the
169 mixed layer depth (see Fig.2f) based on the difference criterion, in which sigma theta changed by
170 0.03 kg/m^3 . The MLD values at the stations along the cruise were later gridded linearly to match
171 the spatial resolution of the underway measurements.

172



173



174
175

176

177

178

179

180

2.2 SOM method and input variables

181

182

183

184

185

186

187

188

189

190

191

192

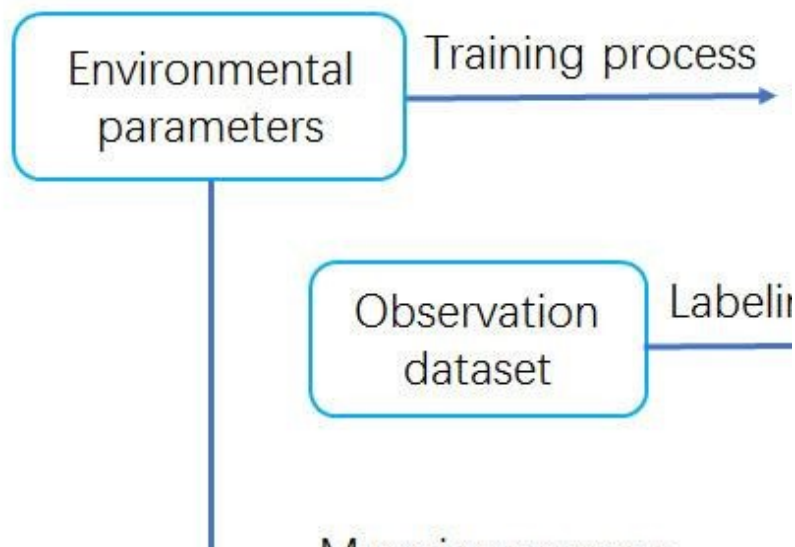
Fig.2 The distributions of underway oceanic and atmospheric $p\text{CO}_2$, SST, SSS, and CHL gridded from MODIS, as well as MLD gridded from station surveys, from February to early March.

We hypothesize that oceanic $p\text{CO}_2$ can be reconstructed using the SOM method with four proxy parameters (Eq. 1): sea surface temperature (SST), chlorophyll-a concentration (CHL), mixed layer depth (MLD), and sea surface salinity (SSS).

$$p\text{CO}_2^{\text{sca}} = \text{SOM}(\text{SST}, \text{CHL}, \text{MLD}, \text{SSS}) \quad (1)$$

The SOM is trained to project the input space of training samples to a feature space (Kohonen, 1984), which is usually represented by grid points in two-dimensional space. Each grid point, which is also called a neuron cell, is associated with a weight vector having the same number of components as the vector of the input data (Zeng et al., 2017). During SOM analysis, three steps are taken following Nakaoka et al. (2013) to estimate the oceanic $p\text{CO}_2$ fields (see Fig. 3). Because the four input environmental parameters (SST, CHL, MLD, and SSS) are used to estimate $p\text{CO}_2$ in this study, each input data set is prepared in 4-D vector form. Here, the SOM analysis was carried out using the MATLAB SOM tool box 2.0 (Vesanto, 2002). It has been developed by the

193 Laboratory of Computer and Information Science in the Helsinki University of Technology and is
 194 available from the following web page: <http://www.cis.hut.fi/projects/somtoolbox>.



195
 196 Fig. 3. Schematic diagram of the main three steps involved in the SOM neural network calculations used to
 197 obtain weekly $p\text{CO}_2$ maps for February to early March of 2015.

198 During the training process, each neuron's weight vectors (P_i), which are linearly initialized,
 199 are repeatedly trained by being presented with the input vectors (Q_j) of environmental parameters
 200 in the SOM training function. Because SOM analysis is known to be a powerful technique with
 201 which to estimate $p\text{CO}_2$ based on the non-linear relationships of the parameters (Telszewski et al.,
 202 2009), we assumed that the non-linear relationships of the proxy parameters are sufficiently
 203 represented after the training procedure. During this step, Euclidean distances (D) are calculated
 204 between the weight vectors of neurons and the input vectors as shown in Eq.2, and the neuron with
 205 the shortest distance is selected as the winner. This process results in the clustering of similar
 206 neurons and the self-organization of the map. The observed oceanic $p\text{CO}_2$ data are not needed in
 207 the first step.

$$D(\mathbf{P}_i; \mathbf{Q}_j) = \sqrt{(P_{i_SST} - Q_{j_SST})^2 + (P_{i_CHL} - Q_{j_CHL})^2 + (P_{i_MLD} - Q_{j_MLD})^2 + (P_{i_SSS} - Q_{j_SSS})^2}$$

208 ... (Eq. 2) During
 209 the second part of the process, each preconditioned SOM neuron is labelled with an observation
 210 dataset of in situ oceanic $p\text{CO}_2$ values, and the labelling process technically follows the same
 211 principles as the training process. The labelling dataset, which consists of the observed $p\text{CO}_2$ and
 212

213 normalized SST, CHL, MLD and SSS data, is presented to the neural network. We calculated the
 214 D values between trained neurons and observational environmental data sets. The winner neuron is
 215 selected as in step1 and labelled with an observed $p\text{CO}_2$ value. After the labelling process, the
 216 neurons are represented as 5-D vectors.

217 Finally, during the mapping process, the labelled SOM neurons created by the second process
 218 and the trained SOM neurons created by the first process are used to produce the oceanic $p\text{CO}_2$
 219 value of each winner neuron based on its geographical grid point in the study area.

220 Before the training process, the input training dataset and labelling dataset are analysed and
 221 prospectively normalized to create an even distribution. The statistics and ranges of the values of
 222 all variables are presented in Table 1. When the datasets of the four proxy parameters were
 223 logarithmically normalized, the skewness values of CHL and MLD changed, especially for the
 224 training dataset. The N coverage represents the percentage of the training data that are labelled.
 225 The data N coverage values of the training data sets of CHL, MLD and SSS are 82.1%, 85% and
 226 81.1%, respectively, which may be due to their insufficient spatiotemporal coverage and/or bias
 227 between the labelling and training data sets. The N coverage of the logarithmic datasets changed to
 228 93.6% and to 98.7% for CHL and MLD, respectively. Thus, the common logarithms of the CHL
 229 and MLD values are used for both the training and labelling datasets to resolve the data coverage
 230 issue arising from significantly increasing the data coverage as well as to overcome the weighting
 231 issue arising from the different magnitudes between variables (Ultsch and Röske, 2002).

232 Table 1. Statistics of labelling and training data sets showing the distribution and coverage of each
 233 variable.

Coverage of each variable		SST[C]	CHL[mg/m ³]	MLD[m]	SSS[psu]
Labelling	Max	0.81	11.13	40.69	33.81
	Min	-1.44	0.17	7.84	32.43
	Mean	-0.27	3.80	14.41	33.27
	Skewness	0.4(-0.2) [#]	0.8(-0.3)	0.9(0.4)	0.6(0.6)
Training	Max	2.48	40.17	48.95	34.17
	Min	-1.8	0.06	10.46	28.64
	Mean	-0.53	1.36	14.79	33.16
	Skewness	0.5(-0.6)	4.3(0.5)	2.6(0.8)	-0.9(-1.0)
	N coverage* (%)	91.3(92.5) ⁺	82.1(93.6)	85.0(98.7)	81.1(80.4)

234 [#] The skewness of the common logarithm of each variable is shown in parentheses.

235 * [number of training data within the labelling data range]/[total number of training data]

236 + The percent labelling data coverage of normalized variables is shown in parentheses

237 In this study, we construct weekly oceanic $p\text{CO}_2$ maps from February to early March of
238 2015 using four datasets, i.e., SST, CHL, MLD, and SSS. Considering the size of our study
239 region, we chose a spatial resolution of 0.1° latitude by 0.1° longitude. For SST, we used daily
240 data from AVHRR ONLY (<https://www.ncdc.noaa.gov/oisst>) with a $1/4^\circ$ spatial resolution (see
241 Fig.S1). CHL data represent the 8-D composite chlorophyll-a data from MODIS-Aqua
242 (<http://oceancolor.gsfc.nasa.gov>) with a spatial resolution of 4 km (see Fig.S2). We also used the
243 daily SSS and MLD data (see Fig.S3-4) from the $1/12^\circ$ global analysis and forecast product from
244 the Copernicus Marine Environment Monitoring Service (CMEMS, <http://marine.copernicus.eu/>).
245 Sea ice concentration data are from the daily 3.125-km AMSR2 dataset (Sprenn et al., 2008,
246 available on <https://seaice.uni-bremen.de>, see Fig.S5).

247 All daily datasets were first averaged to 8-day fields, which are regarded as weekly in this
248 study. The period from the beginning of February to early March comprises four independent
249 week series: week-1 (from 02/02/2015 to 02/09/2015), week-2 (from 02/10/2015 to 02/17/2015),
250 week-3 (from 02/18/2015 to 02/25/2015), and week-4 (from 02/26/2015 to 03/05/2015). The
251 weekly proxy parameters (SCMS) were further re-gridded to a horizontal resolution of $0.1^\circ \cdot 0.1^\circ$
252 using the Kriging method in SURFER software (version 7.3.0.35). In the SOM analyses, input
253 vectors with missing elements are excluded. We compared the assimilated datasets of SST from
254 AVHRR with the in situ measurements obtained by CTD along the cruise. Their correlation is 0.97,
255 and their root-mean-square error (RMSE) is 0.2°C . Comparing the SSS and MLD fields from the
256 Global Forecast system with the in situ measurements yields correlations of 0.76 and 0.74 and
257 RMSEs of 0.41 psu and 5.15 m, respectively. The uncertainty of the MODIS CHL data in the
258 Southern Ocean is approximately 35% (Xu et al., 2016). For the labelling procedure, the observed
259 oceanic $p\text{CO}_2$ together with the corresponding in situ SST, SSS, MLD, and MODIS CHL products
260 in vector form are used as the input dataset.

261 **2.3 Validation of SOM-derived oceanic $p\text{CO}_2$**

262 More realistic $p\text{CO}_2$ estimates are expected from SOM analyses when the distribution and
263 variation ranges of the labelling variables closely reflect those of the training data sets (Nakaoka et
264 al., 2013). However, our underway measurements of $p\text{CO}_2$ values have spatiotemporal limitations
265 preventing them from covering the range of variation of the training data sets. To validate the

266 oceanic $p\text{CO}_2$ values reconstructed by the SOM analysis, we used the fugacity of oceanic CO_2
 267 datasets from the Surface Ocean CO_2 Atlas (hereafter referred to as “SOCAT”
 268 data, <http://www.socat.info>) version 5 database (Bakker et al., 2016). We selected the dataset from
 269 SOCAT (the EXPCODE is 09AR20150128, see cruise in Fig. 4a) that coincided with the same
 270 period as our study. The cruise lasted from Feb. 6 to Feb. 27, 2015, and $f\text{CO}_2$ measurements were
 271 made every 1 min at a resolution of 0.01° . We recalculated $p\text{CO}_2$ values based on the obtained
 272 $f\text{CO}_2$ values provided by the SOCAT data using the fugacity correction (Pfeil et al., 2013).

273

274 **2.4 Carbon uptake in the Prydz Bay**

275 The flux of CO_2 between the atmosphere and the ocean was determined using $\Delta p\text{CO}_2$ and the
 276 transfer velocity across the sea-air interface, as shown in Eq. 3, where K is the gas transfer
 277 velocity (in cm h^{-1}), and the quadratic relationship between wind speed (in units of m s^{-1}) and the
 278 Schmidt number is expressed as $(\text{Sc}/660)^{-0.5}$. L is the solubility of CO_2 in seawater (in mol litre^{-1}
 279 atm^{-1}) (Weiss, 1974). For the weekly estimation in this study, the scaling factor for the gas transfer
 280 rate is changed to 0.25 l for shorter time scales and intermediate wind speed ranges (Wanninkhof,
 281 2014). Considering the unit conversion factor (Takahashi et al., 2009), the weekly sea-air carbon
 282 flux in the Prydz Bay can be estimated using Eq. (4):

$$283 \quad Flux_{\text{sea-air}} = K \times L \times \Delta p\text{CO}_2 \quad (3)$$

$$284 \quad Flux_{\text{sea-air}} [\text{g C}/(\text{m}^2 \cdot \text{week})] = 30.8 \times 10^{-4} \times U^2 \times (p\text{CO}_2^{\text{sea}} - p\text{CO}_2^{\text{air}}) \quad (4)$$

285 where U represents the wind speed 10 m above sea level, and $p\text{CO}_2^{\text{sea}}$ and $p\text{CO}_2^{\text{air}}$ are the partial
 286 pressures of CO_2 in sea water and the atmosphere, respectively.

287 We downloaded weekly ASCAT wind speed data (<http://www.remss.com/>, see Fig. S6)
 288 with a resolution of $1/4^\circ$ and then gridded the dataset to fit the 0.1° longitude \cdot 0.1° latitude spatial
 289 resolution of the SOM-derived oceanic $p\text{CO}_2$. We gridded the atmospheric $p\text{CO}_2$ data collected
 290 along the cruise track to fit the spatial resolution of the SOM-derived oceanic $p\text{CO}_2$ data using a
 291 linear method. The total carbon uptake was then obtained by accumulating the flux of each grid in
 292 each area according to Jiang et al. (2008) and using the proportion of ice-free areas (Takahashi et
 293 al., 2012). When the ice concentration is less than 10% in a grid, we regard the grid box as
 294 comprising all water. When the ice concentration falls between 10% and 90%, the flux is
 295 computed as being proportional to the water area. In the cases of leads or polynyas due to the

296 dynamic motion of sea ice (Worby et al., 2008), we assume the grid box to be 10% open water
297 when the satellite sea ice cover is greater than 90%.

298 **3 Results and discussion**

299 **3.1 The distributions of underway measurements**

300 During austral summer, daylight lasts longer and solar radiation increases. With increasing
301 sea surface temperature, ice shelves break and sea ice melts, resulting in the stratification of the
302 water column. Starting in the beginning of February, the R/V Xuelong sailed from east to west
303 along the sea ice edge, and its underway measurements are shown in Fig.2. Based on the water
304 depth and especially the different ranges of oceanic $p\text{CO}_2$ (see Fig.2a and Table2), the study area
305 can be roughly divided into three regions, namely, the Open-ocean region, Sea-ice region and
306 Shelf region (see Table2).

307 The Open-ocean region ranges northward from 66°S to 64°S, where the Antarctic Divergence
308 Zone is located and water depths are greater than 3000 m. In the Open-ocean region, the oceanic
309 $p\text{CO}_2$ was the highest, varying from 291.98 μatm to 379.31 μatm , with a regional mean value of
310 341.48 μatm . The Antarctic Divergence Zone was characterized by high nutrient concentrations
311 and low chlorophyll concentrations, with high $p\text{CO}_2$ attributed to the upwelling of deep waters,
312 thus suggesting the importance of physical processes in this area (Burkill et al., 1995; Edwards et
313 al., 2004). The underway sea surface temperatures in this region are relatively high, with an
314 average value of -0.23°C due to the upwelling of Circumpolar Deep Water (CDW), while at the
315 sea ice edge (73°E, 65.5°S to 72°E, 65.8°S), the SST decreased to less than -1°C . From 67.5°E
316 westward, affected by the large gyre, cold water from high latitudes lowered the SST to less than
317 0°C . Near the sea ice edge, SSS decreased quickly to 31.7 psu due to the diluted water; along the
318 65°S cruise, it reached 33.3 psu; then, moving westward from 67.5°E, affected by the fresher and
319 colder water brought by the large gyre, it decreased to 32.5 psu. The satellite chlorophyll-a image
320 showed that the regional mean was as low as 0.45 mg/m^3 , except when the vessel near the sea ice
321 edge recorded CHL values that increased to 2.26 mg/m^3 . The lowest $p\text{CO}_2$ value was found near
322 the sea ice edge due to biological uptake. The distribution of MLD varied along the cruise. Near
323 the sea ice edge, because of the melting of ice and direct solar warming, a low-density cap existed
324 over the water column, and the MLD was as shallow as 10.21 m. The maximum value of MLD in
325 the Open-ocean region was 31.67 m. In the Open-ocean region, atmospheric $p\text{CO}_2$ varied from
326 374.6 μatm to 387.8 μatm . Along the 65°E cruise in the eastern part of the Open-ocean region, the

327 oceanic $p\text{CO}_2$ was relatively high, reaching equilibrium with atmospheric $p\text{CO}_2$. In the western
328 part of this region, the oceanic $p\text{CO}_2$ decreased slightly due to the mixture of low $p\text{CO}_2$ from
329 higher latitudes brought by the large gyre. Mixing and upwelling were the dominant factors
330 affecting the oceanic $p\text{CO}_2$ in this region.

331 The seasonal Sea-ice region (from 66°S to 67.25°S) is located between the Open-ocean region
332 and the Shelf region. In this sector, sea ice changed strongly, and the water depth varied sharply
333 from 700 m to 2000 m. The oceanic $p\text{CO}_2$ values ranged from $190.46 \mu\text{atm}$ to $364.43 \mu\text{atm}$, with a
334 regional mean value of $276.48 \mu\text{atm}$. Sea ice continued to change and reform from late February to
335 the beginning of March (Fig. 6). The regional mean sea surface temperature decreased slightly
336 compared to that in the Open-ocean region, and the average value was -0.72°C . With the rapid
337 changes in sea ice, the sea surface temperature and salinity varied sharply from -1.3°C to 0.5°C
338 and from 31.8 psu to 33.3 psu, respectively. When sea ice melted, the water temperature increased,
339 biological activity increased, and the chlorophyll-a value increased slightly to reach a regional
340 average of 0.59 mg/m^3 . Due to the rapid change in sea ice cover, the value of MLD varied from
341 12.8 m to 30.9 m.

342 The Shelf region (from 67.25°S southward) is characterized by shallow depths of less than
343 700 m, and it is surrounded by the Amery Ice Shelf and the West Ice Shelf. Water inside the Shelf
344 region is formed by the modification of low-temperature and high-salinity shelf water (Smith et al.,
345 1984). The Prydz Bay coastal current flows from east to west in the semi-closed bay. The oceanic
346 $p\text{CO}_2$ values in this region were the lowest of those in all three sectors; these values ranged from
347 $151.70 \mu\text{atm}$ to $277.78 \mu\text{atm}$, with a regional average of $198.72 \mu\text{atm}$. A fresher, warmer surface
348 layer is always present over the bay, which is known as the Antarctic Surface Water (ASW).
349 During our study period, the Shelf region was the least ice-covered region. A large volume of
350 freshwater was released into the bay, resulting in low sea surface temperature (an average of
351 -0.61°C) and salinity (an average of 32.4 psu) values. As shown in Fig.2f, the mixed layer depth in
352 most of the inner shelf is low. Due to the vast shrinking of sea ice and strong stratification in the
353 upper water, algal blooming occurred and chlorophyll values were high, with an average of 1.93
354 mg/m^3 . The chlorophyll-a value was remarkably high, reaching 11.04 mg/m^3 when sea ice retreated
355 eastwardly from 72.3°E , 67.3°S to 72.7°E , 68°S . The biological pump became the dominant
356 factor controlling the distribution of oceanic $p\text{CO}_2$. In the bay mouth close to the Fram Bank, due
357 to local upwelling, the water salinity increased remarkably to approximately 33.2 psu.

358 Table2 The regional mean values of underway measurements in three sub-regions

	pCO_2 [μatm]	SST [$^{\circ}$]	CHL [mg/m^3]	MLD [m]	SSS [psu]
Open-ocean region (66°S - 64°S)	341.48	-0.23	0.45	20.13	32.61
Sea-ice region (66°S - 67.25°S)	276.48	-0.72	0.59	19.44	32.42
Shelf region (67.25°S - 70°S)	198.72	-0.61	1.95	16.84	32.46

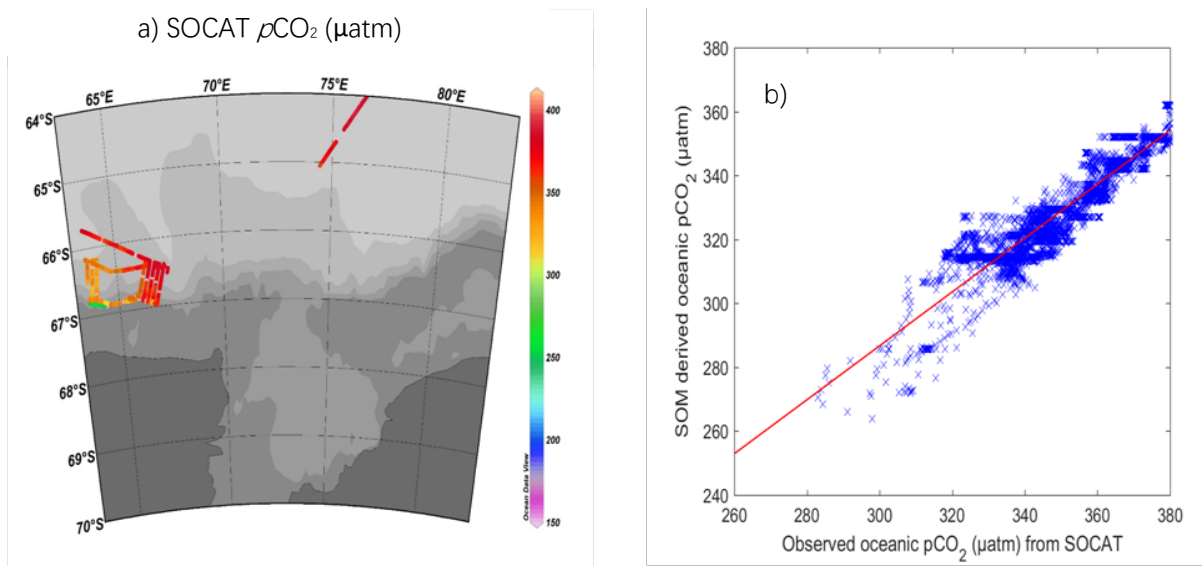
359

360 3.2 Quality and maps of SOM-derived oceanic pCO_2

361 We selected SOM-derived oceanic pCO_2 values to fit the cruise track of SOCAT for the same
 362 period in February 2015 using a nearest-grid method. The RMSE between the SOCAT data and
 363 the SOM-derived result was calculated as follows:

$$364 \quad RMSE = \sqrt{\frac{\sum (pCO_2^{sea}(SOM) - pCO_2^{sea}(SOCAT))^2}{n}} \quad (4)$$

365 where n is the number of validation datasets. The RMSE can be interpreted as an estimation of the
 366 uncertainty in the SOM-derived oceanic pCO_2 in the Prydz Bay. In this study, the RMSE of the
 367 SOM-derived oceanic pCO_2 and SOCAT datasets is 22.14 μatm , and the correlation coefficient
 368 R^2 is 0.82. The absolute mean difference is 23.58 μatm . The RMSE obtained in our study is
 369 consistent with the accuracies (6.9 μatm to 24.9 μatm) obtained in previous studies that used
 370 neuron methods to reconstruct oceanic pCO_2 (Nakaoka et al., 2013; Zeng et al., 2002; Sarma et al.,
 371 2006; Jo Y H et al., 2012; Hales et al., 2012; Telszewshi et al., 2009). The precision of this study is
 372 on the high side of those that have been previously reported. The slope of the scatter plot
 373 indicates that the SOM-derived oceanic pCO_2 data are lower than the SOCAT data (see Fig. 4b).
 374 Thus, the precision of these data may have greater uncertainty because the SOCAT dataset does
 375 not cover the low- pCO_2 area towards the south. Thus, increasing the spatial coverage of the
 376 labelling data will help increase the precision of the SOM-derived oceanic pCO_2 .



377 Fig. 4 a) The cruise lines from SOCAT used to validate the SOM-derived oceanic $p\text{CO}_2$ for the study period in
 378 2015; b) comparison between the SOM-derived and observed SOCAT oceanic $p\text{CO}_2$ data.

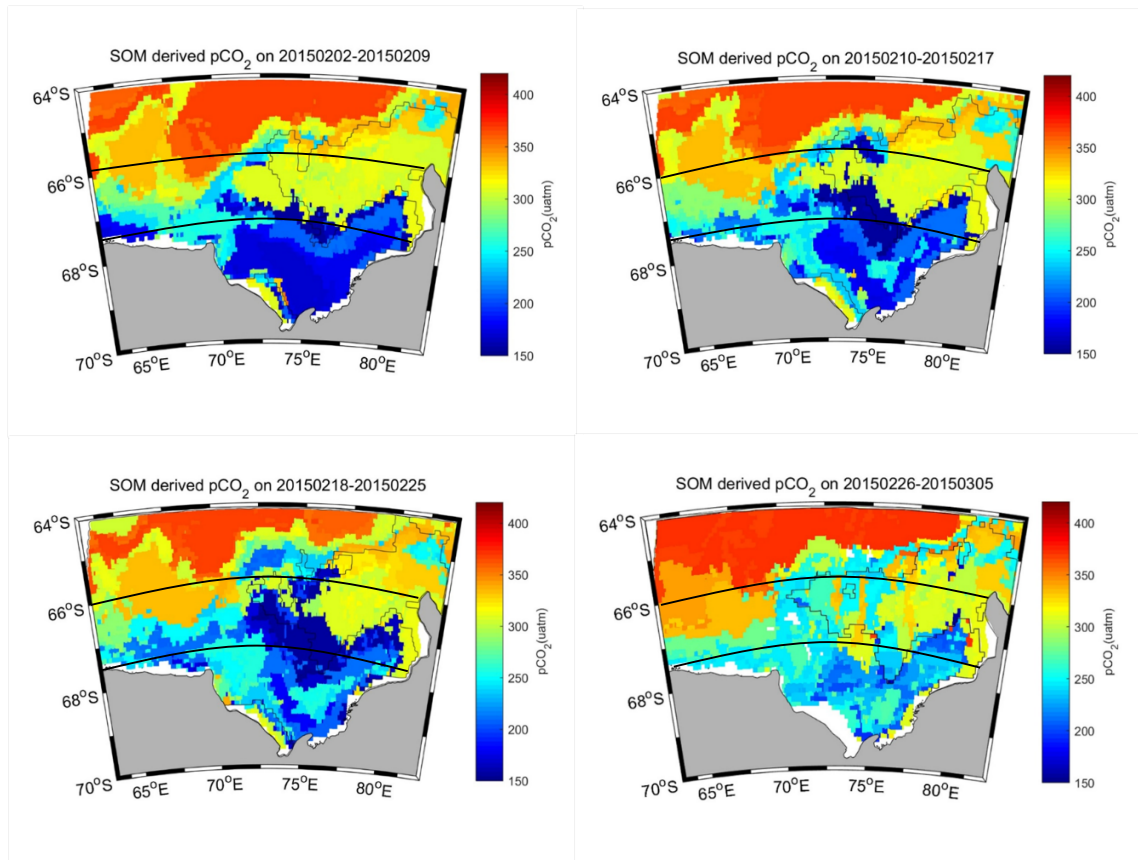
379

380 3.3 Spatial and temporal distributions of SOM-derived oceanic $p\text{CO}_2$

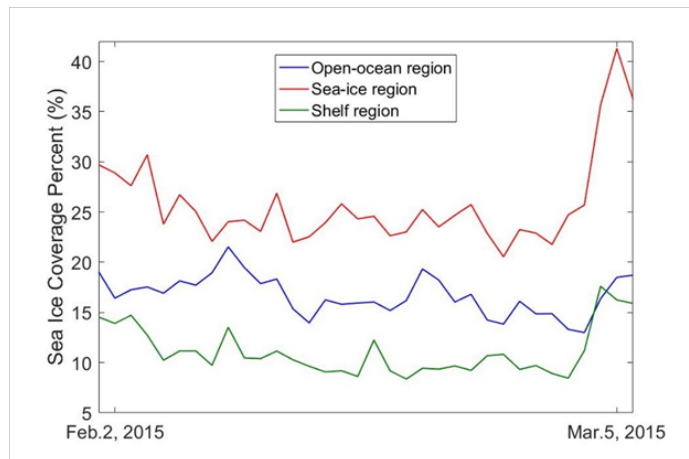
381 The weekly mean maps of SOM-derived oceanic $p\text{CO}_2$ in the Prydz Bay are shown in Fig. 5.
 382 In the Open-ocean region, the oceanic $p\text{CO}_2$ values were higher than those in the other two
 383 regions due to the upwelling of the CDW. During all four weeks, this region was nearly ice-free,
 384 while the average sea ice coverage was 18.14% due to the presence of permanent sea ice (see
 385 Fig.6). The oceanic $p\text{CO}_2$ distribution decreased from east to west in the Open-ocean region,
 386 with lower values observed at the edge of sea ice. In the western part of the Open-ocean region,
 387 oceanic $p\text{CO}_2$ decreased due to mixing with low oceanic $p\text{CO}_2$ flowing from high-latitude regions
 388 caused by the large gyre. From week-1 to week-4, the maximum oceanic $p\text{CO}_2$ increased slightly
 389 and reached 381.42 μatm , which was equivalent to the $p\text{CO}_2$ value of the atmosphere.

390 In the Sea-ice region, sea ice continued to rapidly melt and reform. The weekly mean sea ice
 391 coverage percentage was 29.54%, occupying nearly one-third of the Sea-ice region. As shown in
 392 Fig.5, the gradient of the oceanic $p\text{CO}_2$ distribution increased from south to north affected by the
 393 flow coming from the Shelf region by the large gyre. In the eastern part of this region, adjacent
 394 to the sea ice edge, the oceanic $p\text{CO}_2$ values were lower. The oceanic $p\text{CO}_2$ changed sharply from
 395 155.86 μatm (near the sea ice edge) to 365.11 μatm (close to the Open-ocean region).

396 In austral winter, the entire Prydz Bay basin is fully covered by sea ice, except in a few areas,
397 i.e., the polynyas, which remain open due to katabatic winds (Liu et al., 2017). When the austral
398 summer starts, due to coincident high wind speeds, monthly peak tides, and/or the effect of
399 penetrating ocean swells, the sea ice in the Shelf region starts to melt first in early summer (Lei et
400 al., 2010), forming the Prydz Bay Polynya. The semi-closed polynya functions as a barrier for
401 water exchange in the Shelf region and causes a lack of significant bottom water production,
402 hindering the outflow of continental shelf water and the inflow of Antarctic circle deep water,
403 resulting in the longer residence time of vast melting water and enhanced stratification (Sun et al.,
404 2013). Due to vast melting of the sea ice, the sea surface salinity decreased and algae bloomed;
405 biological productivity promptly increased, and the chlorophyll-a concentration reached its peak
406 value. As shown in Fig. 5, the distribution of oceanic $p\text{CO}_2$ in the Shelf region was characterized
407 by its lowest values. The obvious drawdown of oceanic $p\text{CO}_2$ occurred in the Shelf region due to
408 phytoplankton photosynthesis during this summer bloom. The lowest oceanic $p\text{CO}_2$ in the Shelf
409 region was $153.83 \mu\text{atm}$, except at the edge of the West Ice Shelf, where the Shelf oceanic $p\text{CO}_2$
410 exceeded $300 \mu\text{atm}$. The oceanic $p\text{CO}_2$ was the lowest in week-1, which coincided with a peak in
411 chlorophyll-a, as evidenced by satellite images. The regional oceanic $p\text{CO}_2$ increased slightly in
412 week-4 compared to the other three weeks.



413
 414 Fig.5 Distribution of weekly mean SOM-derived oceanic $p\text{CO}_2$ in the Prydz Bay (unit: μatm) from Feb. 2,
 415 2015 to Mar. 5, 2015. The black contour represents a sea ice concentration of 15%.



416
 417 Fig. 6 Percentage of sea ice coverage in three sub-regions from Feb. 2, 2015 to Mar. 5, 2015 (blue:
 418 Open-ocean region; red: Sea-ice region; green: Shelf region).

419 **3.4 Carbon uptake in the Prydz Bay**

420 During our study period, the entire region was undersaturated, with CO₂ being absorbed
421 by the ocean. The regional averaged ocean-air pCO₂ difference ($\Delta p\text{CO}_2$) was highest in the Shelf
422 region, followed by the Sea-ice region and Open-ocean region (see Table3). The regional and
423 weekly mean $\Delta p\text{CO}_2$ in the Shelf region changed from -184.31 μatm in week-1 to -141.00 μatm in
424 week-2 as chlorophyll decreased. The $\Delta p\text{CO}_2$ in the Sea-ice region and Open-ocean region
425 showed the same patterns, increasing from week-1 to week-3 and then decreasing in week-4.
426 Based on the $\Delta p\text{CO}_2$ and wind speed data, the uptake of CO₂ in these three regions is presented in
427 Table3. The uncertainty of the carbon uptake depends on the errors associated with the wind speed,
428 the scaling factor and the accuracy of the SOM-derived pCO₂ according to Eq.4. The scaling factor
429 will yield a 20% uncertainty in the regional flux estimation. The errors in the wind speeds of the
430 ASCAT dataset are assumed to be 6% (Xu et al., 2016); the error in the quadratic wind speed is
431 12%. The RMSE of the SOM-derived pCO₂ is 22.14 μatm . Considering the errors described above
432 and the uncertainty occurring when the sea-air computation expression is simplified (1.39%, Xu et
433 al., 2016), the total uncertainty of the final uptake is 27%. In the Shelf region, the low oceanic
434 pCO₂ levels drove relatively intensive CO₂ uptake from the atmosphere. The carbon uptake in the
435 Shelf region changed from week-1 (2.51±0.68 TgC, 10¹² gram=Tg) to week-2 (2.77±0.75 TgC).
436 In contrast, in week-3, the wind speed slowed down, resulting in the uptake of CO₂ in the Shelf
437 region decreasing to 2.10±0.57 TgC. In week-4, even though the $\Delta p\text{CO}_2$ was the lowest of all four
438 weeks, the total absorption still increased to 2.63±0.715 TgC due to the high wind speed (with an
439 average value of 7.92 m/s). The total carbon uptake in the three regions of the Prydz Bay,
440 integrated from February to early March of 2015, was 23.57 TgC, with an uncertainty of ±6.36
441 TgC.

442 Table3 Regional and weekly mean $\Delta p\text{CO}_2$, wind speed and uptake of CO₂ in three
443 sub-regions (negative values represent directions moving from air to sea).

		Week-1	Week-2	Week-3	Week-4	Uptake in 4 weeks[Tg]
Open-ocean region (66°S - 64°S)	$\Delta p\text{CO}_2$ [μatm]	-34.11	-42.69	-51.94	-34.08	
	Wind speed [m/s]	7.82	8.54	7.02	9.31	-5.74
	Uptake [Tg]	-1.08	-1.55	-1.51	-1.60	
Sea-ice region (66°S - 67.25°S)	$\Delta p\text{CO}_2$ [μatm]	-115.92	-119.83	-127.74	-86.72	
	Wind speed[m/s]	7.67	8.17	6.39	8.36	-7.82
	Uptake [Tg]	-2.11	-2.35	-1.73	-1.63	
Shelf region (67.25°S - 70°S)	$\Delta p\text{CO}_2$ [μatm]	-184.32	-170.23	-158.61	-141.03	
	Wind speed[m/s]	6.92	7.27	6.67	7.92	-10.01
	Uptake [Tg]	-2.51	-2.77	-2.10	-2.63	

444

445 Roden et al. (2013) estimated the coastal Prydz Bay to be an annual net sink for CO₂ of
446 0.54±0.11 mol/(m²·year), i.e., 1.48±0.3 g/(m²·week). Gibsonab et al. (1999) estimated the average
447 sea-air flux in the summer ice-free period to be more than 30 mmol/(m²·day), i.e., 9.2 g/(m²·week).
448 Our study suggests that the sea-air flux during the strongest period of the year, i.e., February, could
449 be much larger. The average flux obtained here, 18.84 g/(m²·week), is twice as large as the average
450 value estimated over a longer period (November to February) reported by Gibsonab et al. (1999).

451 As the region recording the strongest surface unsaturation of these three regions in summer,
452 the Shelf region has a potential carbon uptake of 10.01±2.7 Tg C from February to early March,
453 which accounts for approximately 5.0‰-6.7‰ of the net global ocean CO₂ uptake according to
454 Takahashi et al. (2009), even though its total area is only 78*10³ km². Due to the sill constraint,
455 there is limited exchange between water masses in and outside the Prydz Bay. During winter, the
456 dense water formed by the ejection of brine in the Bay can potentially uptake more anthropogenic
457 CO₂ from the atmosphere that can descend to greater depths, thus enhancing the acidification in
458 deep water. According to Shadwick et al. (2013), the winter values of *p*H and Ω decrease more
459 remarkably than those in summer. As the bottom water in the Prydz Bay is a possible source of
460 Antarctic Bottom Water (Yabuki et al., 2006), the Shelf region may transfer anthropogenic CO₂ at
461 the surface to deep water and may thus influence the acidification of the deep ocean over long
462 timescales.

463

464 **4 Summary**

465 Based on the different observed ranges of the distribution of ocean *p*CO₂, the Prydz Bay
466 region was divided into three sectors from February to early March of 2015. In the Shelf region,
467 biological factors exerted the main control on oceanic *p*CO₂, while in the Open-ocean region,
468 mixing and upwelling were the main controls. In the Sea-ice region, due to rapid changes in sea ice,
469 oceanic *p*CO₂ was controlled by both biological and physical processes. SOM is an important tool
470 for the quantitative assessment of oceanic *p*CO₂ and its subsequent sea-air carbon flux, especially
471 in dynamic, high-latitude, and seasonally ice-covered regions. The estimated results revealed that
472 the SOM technique can be used to reconstruct the variations in oceanic *p*CO₂ associated with
473 biogeochemical processes expressed by the variability in four proxy parameters: SST, CHL, MLD
474 and SSS. The RMSE of the SOM-derived oceanic *p*CO₂ is 22.14 μatm for the SOCAT dataset.

475 From February to early March of 2015, the Prydz Bay region was a strong carbon sink, with a
476 carbon uptake of 23.57 ± 6.36 TgC. The strong potential uptake of anthropogenic CO₂ in the Shelf
477 region will enhance the acidification in the deep water region of the Prydz Bay and may thus
478 influence the acidification of the deep ocean in the long run because it contributes to the formation
479 of Antarctic Bottom Water.

480 **Acknowledgments**

481 This work is supported by National Natural Science Foundation of China
482 (NSFC41506209, 41630969, 41476172, 41230529), Qingdao National Laboratory for marine
483 science and technology (QNLM2016ORP0109), Chinese Projects for Investigations and
484 Assessments of the Arctic and Antarctic (CHINARE2012-2020 for 01-04, 02-01, and 03-04). This
485 work is also supported by Korea Polar Research Institute grants PE18060 and PE18070. We would
486 like to thank China Scholarship Council (201704180019) and State Administration of Foreign
487 Experts Affairs P. R. China for their support in this research. We would like to thank the carbon
488 group led by Zhongyong Gao and Heng Sun in GCMAC and the crew on R/V Xuelong for their
489 support on the cruise. We are thankful to contributors of the SOCAT database for validated *p*CO₂
490 data and Mercator Ocean for providing the Global Forecast model output. We deeply appreciate
491 Dr. Xianmin Hu in Bedford Institute of Oceanography, who provided us with useful technical
492 instructions.

493 **References**

- 494
- 495 1. Bakker, D. C. E., Pfeil, B. Landa, C. S., Metzl, N., O'Brien, K. M., Olsen, A., Smith, K.,
496 Cosca, C., Harasawa, S., Jones, S. D., Nakaoka, S., Nojiri, Y., Schuster, U., Steinhoff, T.,
497 Sweeney, C., Takahashi, T., Tilbrook, B., Wada, C., Wanninkhof, R., Alin, S. R., Balestrini,
498 C. F., Barbero, L., Bates, N. R., Bianchi, A. A., Bonou, F., Boutin, J., Bozec, Y., Burger, E.
499 F., Cai, W.-J., Castle, R. D., Chen, L., Chierici, M., Currie, K., Evans, W., Featherstone, C.,
500 Feely, R. A., Fransson, A., Goyet, C., Greenwood, N., Gregor, L., Hankin, S.,
501 Hardman-Mountford, N. J., Harlay, J., Hauck, J., Hoppema, M., Humphreys, M. P., Hunt, C.
502 W., Huss, B., Ibáñez, J. S. P., Johannessen, T., Keeling, R., Kitidis, V., Körtzinger, A.,
503 Kozyr, A., Krasakopoulou, E., Kuwata, A., Landschützer, 3P., Lauvset, S. K., Lefèvre, N.,
504 Lo Monaco, C., Manke, A., Mathis, J. T., Merlivat, L., Millero, F. J., Monteiro, P. M. S.,
505 Munro, D. R., Murata, A., Newberger, T., Omar, A. M., Ono, T., Paterson, K., Pearce, D.,

- 506 Pierrot, D., Robbins, L. L., Saito, S., Salisbury, J., Schlitzer, R., Schneider, B., Schweitzer,
507 R., Sieger, R., Skjelvan, I., Sullivan, K. F., Sutherland, S. C., Sutton, A. J., Tadokoro, K.,
508 Telszewski, M., Tuma, M., Van Heuven, S. M. A. C., Vandemark, D., Ward, B., Watson, A.
509 J., and Xu, S.: A multi-decade record of high quality $f\text{CO}_2$ data in version 3 of the Surface
510 Ocean CO_2 Atlas (SOCAT). *Earth System Science Data* 8:
511 383-413.doi:10.5194/essd-8-383-2016, 2016.
- 512 2. Barbini, R., Fantoni, R., Palucci, A., Colao, F., Sandrini, S., Ceradini, S., Tositti, L.,
513 Tubertini, O., and Ferrari, G. M.: Simultaneous measurements of remote lidar chlorophyll
514 and surface CO_2 distributions in the Ross Sea. *International Journal of Remote Sensing*, 24,
515 3807-3819, 2003.
- 516 3. Bates, N. R., Hansell, D. A., Carlson, C. A., and Gordon, L. I.: Distribution of CO_2 species,
517 estimates of net community production, and air–sea CO_2 exchange in the Ross Sea polynya,
518 *Journal of Geophysical Research*, 103, 2883-2896, 1998a.
- 519 4. Bates, N. R., Takahashi, T., Chipman, D. W., and Knapp, A. H.: Variability of $p\text{CO}_2$ on diel
520 to seasonal time scales in the Sargasso Sea, *Journal of Geophysical Research*, 103,
521 15567-15585, 1998b.
- 522 5. Brainerd, K. E., and Gregg, M. C.: Surface mixed and mixing layer depth, *Deep Sea Res.*,
523 part A, 42, 1521-1543, 1995.
- 524 6. Burkill, P. H., Edwards, E. S., and Sleight, M. A.: Microzooplankton and their role in
525 controlling phytoplankton growth in the marginal ice zone of the Bellingshausen Sea, *Deep*
526 *Sea Research Part II: Topical Studies in Oceanography*, 42(4), 1277-1290, 1995.
- 527 7. Chen, L., Xu, S., Gao, Z., Chen, H., Zhang, Y., Zhan, J., and Li, W.: Estimation of monthly
528 air-sea CO_2 flux in the southern Atlantic and Indian Ocean using in-situ and remotely sensed
529 data, *Remote Sensing of Environment*, 115(8), 1935-1941, 2011.
- 530 8. Chierici, M., Olsen, A., Johannessen, T., Trinanes, J., and Wanninkhof, R.: Algorithms to
531 estimate the carbon dioxide uptake in the northern North Atlantic using ship-observations,
532 satellite and ocean analysis data, *Deep-Sea Res. Pt. II*, 56(8-10), 630-639, 2009.
- 533 9. Chu, P. C., and Fan, C.: Optimal linear fitting for objective determination of ocean mixed
534 layer depth from glider profiles, *Journal of Atmospheric and Oceanic Technology*, 27(11):
535 1893-1989, 2010.
- 536 10. Dandonneau, Y.: Sea-surface partial pressure of carbon dioxide in the eastern equatorial

- 537 Pacific (August 1991 to October 1992): A multivariate analysis of physical and biological
538 factors, *Deep Sea Research II*, 42(2-3), 349-364, 1995.
- 539 11. Dong, S., Sprintall, J., Gille, S. T., and Talley, L.: Southern Ocean mixed-layer depth from
540 Argo float profiles, *Journal of Geophysical Research*, 113, C06013, doi:
541 10.1029/2006JC004051, 2008.
- 542 12. Edwards, A. M., Platt, T., and Sathyendranath, S.: The high-nutrient, low-chlorophyll
543 regime of the ocean: limits on biomass and nitrate before and after iron enrichment,
544 *Ecological Modelling*, 171, 103-125, 2004.
- 545 13. Friedrich, T., and Oschlies, A.: Basin-scale $p\text{CO}_2$ maps estimated from ARGO float data: A
546 model study, *J. Geophys. Res.*, 114, C10012, doi:10.1029/2009JC005322, 2009b.
- 547 14. Friedrich, T., and Oschlies, A.: Neural network-based estimates of North Atlantic surface
548 $p\text{CO}_2$ from satellite data: A methodological study, *J. Geophys. Res.*, 114, C03020,
549 doi:10.1029/2007JC004646, 2009a.
- 550 15. Gao, Z., Chen, L., and Gao, Y.: Air-sea carbon fluxes and their controlling factors in the
551 Prydz Bay in the Antarctic, *Acta Oceanologica Sinica*, 3(27), 136-146, 2008.
- 552 16. Gibson, P. B., Perkins-Kirkpatrick, S. E., Uotila, P., Pepler, A. S., and Alexander, L. V.: On
553 the use of self-organizing maps for studying climate extremes, *Journal of Geophysical*
554 *Research: Atmospheres*, 122, 3891-3903, 2017.
- 555 17. Gibson, J. A.E., and Trull, T. W.: Annual cycle of $f\text{CO}_2$ under sea-ice and in open
556 water in Prydz Bay, east Antarctica, *Marine Chemistry*, Volume 66, Issues 3-4, 187-200,
557 1999.
- 558 18. Hales, B., Strutton, P., Saraceno, M., Letelier, R., Takahashi, T., Feely, R., Sabine, C., and
559 Chavez, F.: Satellite-based prediction of $p\text{CO}_2$ in coastal waters of the eastern North Pacific,
560 *Progress in Oceanography*, 103, 1-15, 2012.
- 561 19. Hardman-Mountford, N., Litt, E., Mangi, S., Dye, S., Schuster, U., Bakker, D., and Watson,
562 A.: Ocean uptake of carbon dioxide (CO_2), MCCIP BriefingNoteswww.mccip.org.uk, 9pp,
563 2009.
- 564 20. Heil, P., Allison, I. and Lytle, V. I.: Seasonal and interannual variations of the oceanic heat
565 flux under a landfast Antarctic sea ice cover, *J. Geophys. Res.*, 101(C11), 25,741-25,752,
566 doi: 10.1029/96JC01921, 1996.
- 567 21. Huang, J., Xu, F., Zhou, K., Xiu, P., and Lin, Y.: Temporal evolution of near-surface

568 chlorophyll over cyclonic eddy lifecycles in the southeastern Pacific, *Journal of Geophysical*
569 *Research: Oceans* 122, 6165-6179, 2017a.

570 22. Huang, W., Chen, R., Yang, Z., Wang, B., and Ma, W.: Exploring the combined effects of
571 the Arctic Oscillation and ENSO on the wintertime climate over East Asia using
572 self-organizing maps, *Journal of Geophysical Research: Atmospheres*, 122, 9107-9129,
573 2017b.

574 23. Iskandar, I.: Seasonal and interannual patterns of sea surface temperature in Banda Sea as
575 revealed by self-organizing map, *Continental Shelf Research*, 30, 1136-1148, 2010.

576 24. Jacobs, S. S. and Georgi, D. T.: Observations on the south-west Indian/Antarctic Ocean, In
577 *A Voyage of Discovery*, ed. by M. Angel, *Deep-Sea Res.*, 24(suppl.), 43-84, 1977.

578 25. Jamet, C., Moulin, C., and Lefèvre, N.: Estimation of the oceanic $p\text{CO}_2$ in the North Atlantic
579 from VOS lines in situ measurements: Parameters needed to generate seasonally mean maps,
580 *Ann. Geophys.*, 25, 2247-2257, 2007, <http://www.ann-geophys.net/25/2247/2007/>.

581 26. Jiang, L. Q., Cai, W. J., Wanninkhof, R., Wang, Y., and Lüger, H.: Air-sea CO_2 fluxes on
582 the U.S. South Atlantic Bight: Spatial and seasonal variability, *Journal of Geophysical*
583 *Research*, 113 (2008), C07019, doi:10.1029/2007JC004366, 2008.

584 27. Jo, Y. H., Dai, M. H., Zhai, W. D., Yan, X. H., and Shang, S. L.: On the variations of sea
585 surface $p\text{CO}_2$ in the northern South China sea: A remote sensing based neural network
586 approach, *Journal of Geophysical Research*, 117, C08022, doi:10.1029/2011JC007745,
587 2012.

588 28. Kohonen, T.: *Self-Organization and Associative Memory*, Springer, Berlin, 1984.

589 29. Lafevre, N., Watson, A. J., and Watson, A. R.: A comparison of multiple regression and
590 neural network techniques for mapping in situ $p\text{CO}_2$ data, *Tellus B*, 57(5), 375-384, 2005.

591 30. Laruelle, G. G., Landschützer, P., Gruber, N., Tison, J. L., Delille, B., and Regnier, P.:
592 Global high resolution monthly $p\text{CO}_2$ climatology for the coastal ocean derived from neural
593 network interpolation, *Biogeosciences*, 14, 4545-4561, 2017.

594 31. Lei, R., Li, Z., Cheng, B., Zhang, Z., and Heil, P.: Annual cycle of landfast sea ice in Prydz
595 Bay, East Antarctica, *Journal of Geophysical Research Atmospheres*, 115(C2), C02006,
596 doi:10.1029/2008JC005223, 2010.

597 32. Liu C., Wang Z., Cheng C., Xia R., Li B., and Xie Z.: Modeling modified circumpolar deep
598 water intrusions onto the Prydz Bay continental shelf, East Antarctica, *Journal of*

- 599 Geophysical Research, Vol. 122, Issue 7, 5198-5217. DOI: 10.1002/2016JC012336, 2017.
- 600 33. Liu, Y., Weisberg, R. H., and He, R.: Sea Surface Temperature Patterns on the West Florida
601 Shelf Using Growing Hierarchical Self-Organizing Maps, *Journal of Atmospheric and*
602 *Oceanic Technology*, 23, 325-338, 2006.
- 603 34. Liu, Z. L., Ning, X. R., Cai, Y. M., Liu, C. G., and Zhu, G. H.: Primary productivity and
604 chlorophyll a in the surface water on the route encircling the Antarctica during austral
605 summer of 1999/2000, *Polar Research*, 112(4), 235-244, 2000.
- 606 35. Liu, Z., and Cheng Z.: The distribution feature of size-fractionated chlorophyll a and
607 primary productivity in Prydz Bay and its north sea area during the austral summer, *Chinese*
608 *Journal of Polar Science*, 14(2): 81-89, 2003.
- 609 36. Lüger, H., Wallace, D. W. R., Körtzinger, A., and Nojiri, Y.: The $p\text{CO}_2$ variability in the
610 midlatitude North Atlantic Ocean during a full annual cycle, *Global Biogeochem. Cycles*,
611 18, GB3023, doi:10.1029/2003GB002200, 2004.
- 612 37. Metzl, N., Brunet, C., Jabaud-Jan, A., Poisson, A., and Schauer, B.: Sumer and winter
613 air-sea CO_2 fluxes in the Southern Ocean, *Deep-Sea Research*, 153: 1548-1563, 2006.
- 614 38. Middleton, J. H., and Humphries, S. E.: Thermohaline structure and mixing in the region of
615 Prydz Bay, Antarctica, *Deep Sea Research Part A, Oceanographic Research Papers*, 36(8),
616 1255-1266, 1989.
- 617 39. Morrison, J. M., Gaurin, S., Codispoti, L. A., Takahashi, T., Millero, F. J., Gardner, W. D.,
618 and Richardson, M. J.: Seasonal evolution of hydrographic properties in the Antarctic
619 circumpolar current at 170W during 1997-1998, *Deep-Sea Research*, 148: 3943-3972, 2001.
- 620 40. Nakaoka, S., Telszewski, M., Nojiri, Y., Yasunaka, S., Miyazaki, C., Mukai, H., and Usui,
621 N.: Estimating temporal and spatial variation of ocean surface $p\text{CO}_2$ in the North Pacific
622 using a self-organizing map neural network technique, *Biogeosciences*, 10, 6093-6106,
623 2013.
- 624 41. Nunes Vaz, R. A., and Lennon, G. W.: Physical oceanography of the Prydz Bay region of
625 Antarctic waters, *Deep Sea Research Part I: Oceanography Research Papers*, 43(5), 603-641,
626 1996.
- 627 42. Olsen, A., Trinanes, J. A., and Wanninkhof, R.: Sea-air flux of CO_2 in the Caribbean Sea
628 estimated using in situ and remote sensing data, *Remote Sens. Environ.*, 89, 309-325, 2004.
- 629 43. Pfeil, B., Olsen, A., Bakker, D. C. E., Hankin, S., Koyuk, H., Kozyr, A., Malczyk, J.,

- 630 Manke, A., Metzl, N., Sabine, C. L., Akl, J., Alin, S. R., Bellerby, R. G. J., Borges, A.,
631 Boutin, J., Brown, P. J., Cai, W.-J., Chavez, F. P., Chen, A., Cosca, C., Fassbender, A. J.,
632 Feely, R. A., González-Dávila, M., Goyet, C., Hardman- Mountford, N., Heinze, C., Hood,
633 M., Hoppema, M., Hunt, C. W., Hydes, D., Ishii, M., Johannessen, T., Jones, S. D., Key, R.
634 M., Körtzinger, A., Landschützer, P., Lauvset, S. K., Lefèvre, N., Lenton, A., Lourantou, A.,
635 Merlivat, L., Iidorikawa, T., Mintrop, L., Miyazaki, C., Murata, A., Nakadate, A., Nakano,
636 Y., Nakaoka, Y. Nojiri, A. M. Omar, X. A. Padin, G.-H. Park, K. Paterson, F. F. Perez, S.,
637 Pierrot, D., Poisson, A., Ríos, A. F., Salisbury, J., Santana-Casiano, J. M., Sarma, V. V. S.
638 S., Schlitzer, R., Schneider, B., Schuster, U., Sieger, R., Skjelvan, I., Steinhoff, T., Suzuki,
639 T., Takahashi, T., Tedesco, K., Telszewski, M., Thomas, H., Tilbrook, B., Tjiputra, J.,
640 Vandemark, D., Veness, T., Wanninkhof, R., Watson, A. J., Weiss, R., Wong, C. S., and
641 Yoshikawa-Inoue, H.: A uniform, quality controlled Surface Ocean CO₂ Atlas (SOCAT),
642 Earth Syst. Sci. Data, 5, 125-143, doi:10.5194/essd-5-125-2013, 2013.
- 643 44. Pierrot, D., Neill, C., Sullivan, L., Castle, R., Wanninkhof, R., Lüger, H., Johannessen, T.,
644 Olsen, A., Feely, R. A., and Cosca, C. E.: Recommendations for autonomous underway
645 *p*CO₂ measuring systems and data-reduction routines, Deep-Sea Research Part II, 56,
646 512-522, 2009.
- 647 45. Rangama, Y., Boutin, J., Etcheto, J., Merlivat, L., Takahashi, T., Delille, B., Frankignoulle,
648 M., and Bakker, D. C. E.: Variability of the net air-sea CO₂ flux inferred from shipboard and
649 satellite measurements in the Southern Ocean south of Tasmania and New Zealand, Journal
650 of Geophysical Research: Oceans (1978-2012), 110(C9), doi: 10.1029/2004JC002619, 2005.
- 651 46. Roden, N. P., Shadwick, E. H., Tilbrook, B., and Trull, T. W.: Annual cycle of carbonate
652 chemistry and decadal change in coastal Prydz Bay, East Antarctica, Marine Chemistry,
653 155(4), 135-147, 2013.
- 654 47. Rubin, S.I., Takahashi, T., and Goddard, J.G.: Primary productivity and nutrient utilization
655 ratios in the Pacific sector of the Southern Ocean based on seasonal changes in seawater
656 chemistry, Deep-Sea Research I 45, 1211-1234, 1998.
- 657 48. Sabine, L., Feely, R. A., Gruber, N., Key, R. M., Lee, K., Bullister, J. L., Wanninkhof, R.,
658 Wong, S., Wallace, D. W. R., Tilbrook, B., Millero, F. J., Peng, T.-H., Kozyr, A., Ono, T.,
659 and Rios, A. F.: The oceanic sink for anthropogenic CO₂, Science, 305, 367-371,
660 doi:10.1126/science.1097403, 2004.

- 661 49. Sarma, V. V. S. S., Saino, T., Sasaoka, K., Nojiri, Y., Ono, T., Ishii, M., Inoue, H. Y., and
662 Matsumoto, K.: Basin-scale $p\text{CO}_2$ distribution using satellite sea surface temperature, Chla,
663 and climatological salinity in the North Pacific in spring and summer, *Global*
664 *Biogeochemical Cycles*, 20, GB3005, doi:10.1029/2005GB002594, 2006.
- 665 50. Shadwick, E. H., Trull, T. W., Thomas, H., and Gibson, J. A. E.: Vulnerability of polar
666 oceans to anthropogenic acidification: comparison of Arctic and Antarctic seasonal cycles,
667 *Scientific Reports*, 3: 2339, doi: 10.1038/srep02339, 2013.
- 668 51. Silulwane, N. F., Richardson, A. J., Shillington, F. A., and Mitchell-Innes, B. A.:
669 Identification and classification of vertical chlorophyll patterns in the Benguela upwelling
670 system and Angola-Benguela front using an artificial neural network, *South African Journal*
671 *of Marine Science*, 23, 37-51, 2001.
- 672 52. Smith, N. R., Zhaoqian, D., Kerry, K. R., and Wright, S.: Water masses and circulation in
673 the region of Prydz Bay Antarctica, *Deep-sea-research*, 31, 1121-1147, 1984.
- 674 53. Smith, N., and Tréguer, P.: *Physical and chemical oceanography in the vicinity of Prydz*
675 *Bay, Antarctica*, Cambridge University Press, Cambridge, 1994.
- 676 54. Spreen, G., Kaleschke, L., and Heygster, G.: Sea ice remote sensing using AMSR-E 89
677 GHz channels, *J. Geophys. Res.*, 113, C02S03, doi:10.1029/2005JC003384, 2008.
- 678 55. Sun, W. P., Han, Z. B., Hu, C. Y., and Pan, J. M.: Particulate barium flux and its relationship
679 with export production on the continental shelf of Prydz Bay, east Antarctica, *Marine*
680 *Chemistry*, 157, 86-92, 2013.
- 681 56. Sweeney, C., Hansell, D. A., Carlson, C. A., Codispoti, L. A., Gordon, L. I., Marra, J.,
682 Millero, F. J., Smith, W. O., and Takahashi, T.: Biogeochemical regimes, net community
683 production and carbon export in the Ross Sea, Antarctica, *Deep Sea Research II*, 47(15-16),
684 3369-3394, 2000.
- 685 57. Sweeney, C.: The annual cycle of surface water CO_2 and O_2 in the Ross Sea: a model for gas
686 exchange on the continental shelves of Antarctic, *Biogeochemistry of the Ross Sea*,
687 *Antarctic Research Series*, 78, 295-312, 2002.
- 688 58. Sweeney, C.: The annual cycle of surface water CO_2 and O_2 in the Ross Sea: A model for
689 gas exchange on the continental shelves of Antarctic, *Biogeochemistry of the Ross Sea*,
690 *Antarctic Research Series*, 78, 295-312, 2002.

- 691 59. Takahashi, T. Feely, R. A., Weiss, R. F., Wanninkhof, R. H., Chipman, D. W., Sutherland, S.
692 C., and Takahashi, T. T.: Global sea air CO₂ flux based on climatological surface ocean
693 *p*CO₂, and seasonal biological and temperature effects, *Deep-Sea Res. Pt. II*, 49(9-10),
694 1601-1622, 2002.
- 695 60. Takahashi, T., Sutherland, S. C., Wanninkhof, R., Sweeney, C., Feely, R. A., Chipman, D.
696 W., Hales, B., Friederich, G., Chavez, F., Sabine, C., Watson, A. J., Bakker, D. C., Schuster,
697 U., Metzl, N., Yoshikawa-Inoue, H., Ishii, M., Midorikawa, T., Nojiri, Y., Körtzinger, A.,
698 Steinhoff, T., Hoppema, M., Olafsson, J., Arnarson, T. S., Tilbrook, B., Johannessen, T.,
699 Olsen, A., Bellerby, R., Wong, C. S., Delille, B., Bates, N. R., and de Baar, H. J. W.:
700 Climatological mean and decadal change in surface ocean *p*CO₂, and net sea-air CO₂ flux
701 over the global oceans, *Deep-Sea Res. Pt. II*, 56(8-10), 554-577, 2009.
- 702 61. Takahashi, T., Sweeney, C., Hales, B., Chipman, D. W., Newberger, T., Goddard, J. G.,
703 Iannuzzi, R. A., and Sutherland, S. C.: The changing carbon cycle in the Southern Ocean,
704 *Oceanography*, 25, 26-37, 2012.
- 705 62. Telszewski, M., Chazottes, A., Schuster, U., Watson, A. J., Moulin, C., Bakker, D. C. E.,
706 González-Dávila, M., Johannessen, T., Körtzinger, A., Lüger, H., Olsen, A., Omar, A.,
707 Padin, X. A., Ríos, A. F., Steinhoff, T., Santana-Casiano, M., Wallace, D. W. R., and
708 Wanninkhof, R.: Estimating the monthly *p*CO₂ distribution in the North Atlantic using a
709 self-organizing neural network, *Biogeoscience*, 6, 1405-1421, 2009.
- 710 63. Thomson, R. E., and Fine, I. V.: Estimating mixed layer depth from oceanic profile data, *J.*
711 *Atmos. Oceanic Technol.*, 20, 319-329, 2003.
- 712 64. Ultsch, A., and Röske, F.: Self-organizing feature maps predicting sea levels, *Information*
713 *Sciences*, 144, 91-125, 2002.
- 714 65. Vesanto, J.: *Data Exploration Process Based on the Self-Organizing Map: the Finnish*
715 *Academies of Technology*, 2002.
- 716 66. Wanninkhof, R.: Relationship between wind speed and gas exchange over the ocean
717 revisited, *Limnology and Oceanography: Methods*, 12, 351-362, 2014.
- 718 67. Weiss, R. F.: Carbon dioxide in water and seawater: The solubility of a nonideal gas, *Marine*
719 *Chemistry*, 2, 201-215, 1974.
- 720 68. Worby, A. P., Geiger, C. A., Paget, M. J., Van Woert, M. L., Ackley, S. F., and De Liberty,
721 T. L.: Thickness distribution of Antarctic sea ice, *Journal of Geophysical Research* 113,

- 722 C05S92, <http://dx.doi.org/10.1029/2007JC004254>, 2008.
- 723 69. Wu, L., Wang, R., Xiao, W., Ge, S., Chen, Z., and Krijgsman, W.: Productivity-climate
724 coupling recorded in Pleistocene sediments off Prydz Bay (East Antarctica),
725 *Palaeogeography, Palaeoclimatology, Palaeoecology*, 485, 260-270, 2017.
- 726 70. Xu, S., Chen, L., Chen, H., Li, J., Lin, W., and Qi, D.: Sea-air CO₂ fluxes in the Southern
727 Ocean for the late spring and early summer in 2009, *Remote Sensing of Environment*, 175,
728 158-166, 2016.
- 729 71. Yabuki, T., Suga, T., Hanawa, K., Matsuoka, K., Kiwada, H., and Watanabe, T.: Possible
730 source of the Antarctic Bottom Water in Prydz Bay region, *Journal of Oceanography*, 62,
731 649-655, doi: 10.1007/s10872-006-0083-1, 2006.
- 732 72. Zeng, J., Nojiri, Y., Nakaoka, S., Nakajima, H., and Shirai, T.: Surface ocean CO₂ in
733 1990-2011 modelled using a feed-forward neural network, *Geoscience Data Journal*, 2,
734 47-51, doi: 10.1002/gdj3.26, 2015.
- 735 73. Zeng, J., Mtsunaga, T., Saigusa, N., Shirai, T., Nakaoka, S., and Tan, Z.: Technical note:
736 Evaluation of three machine learning models for surface ocean CO₂ mapping, *Ocean Sci.*,
737 13, 303-313, <http://doi.org/10.5194/os-13-303-2017>, 2017.
- 738 74. Zeng, J., Nojiri, Y., Murphy, P. P., Wong, C. S., and Fujinuma, Y.: A comparison of
739 $\Delta p\text{CO}_2$ distributions in the northern North Pacific using results from a commercial vessel in
740 1995-1999, *Deep Sea Res., Part II*, 49, 5303-5315, 2002.
- 741